Chemosphere 294 (2022) 133693

Contents lists available at ScienceDirect

Chemosphere

journal homepage: www.elsevier.com/locate/chemosphere

# Size segregated ionic species collected in a harbour area

B. Navarro-Selma [a], A. Clemente [a], J.F. Nicolás [a], J. Crespo [a], A. Carratalá [b], F. Lucarelli [c], F. Giardi [c], N. Galindo [a], E. Yubero [a,*]

[a] Atmospheric Pollution Laboratory (LCA), Department of Applied Physics, Miguel Hernández University, Avenida de la Universidad S/N, 03202, Elche, Spain
[b] Department of Chemical Engineering, University of Alicante, P. O. Box 99, 03080, Alicante, Spain
[c] Department of Physics and Astronomy, University of Florence and INFN, 50019, Florence, Italy

## HIGHLIGHTS

- Aerosol size distributions in a port environment has been studied.
- The possible origin of particle size distributions of inorganic ions is explained.
- The impact of port activities on aerosol size distributions is analysed.
- Seasonal changes of aerosol size distributions are evaluated.

## GRAPHICAL ABSTRACT

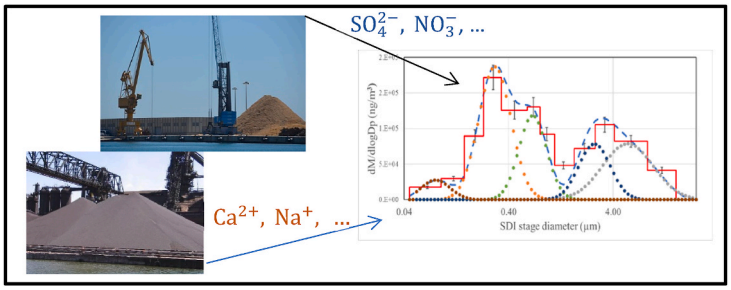


## ARTICLE INFO

Handling Editor: Volker Matthias

*Keywords:*
Port
Bulk materials
Aerosol size distributions
Ionic composition
Harbour emissions

## ABSTRACT

Water-soluble ions were analysed in size segregated aerosol samples collected in the port of Alicante (Southeastern Spain) during summer and winter using a multistage cascade impactor. Seasonal variations in the size distributions of the analysed components and the influence of bulk materials handling (loading/unloading and stockpiling) at the docks were investigated. The size distributions of $SO_4^{2-}$, $NH_4^+$ and $K^+$ were characterized by prominent peaks in the condensation and droplet modes, both in summer and winter, while those of $Ca^{2+}$, $Na^+$, $Mg^{2+}$ and $Cl^-$ had a main peak centred at ~4 μm. Although oxalate size distributions were similar during both seasons, the fraction of coarse-mode oxalate increased in summer most likely as a result of volatilization and repartition processes or reactions of oxalic acid with coarse alkaline particles. Nitrate size distributions were dominated by a coarse mode; however, during winter, modal peaks in the submicron size range were also observed due to favourable conditions for the formation of fine-mode $NH_4NO_3$. Harbour activities had a significant impact only on the concentrations of calcium, particularly in the coarse fraction, during both summer and winter.

## 1. Introduction

Atmospheric aerosol is a complex mixture of inorganic substances and hundreds of different organic compounds (Seinfeld and Pandis, 2016). In the last decades, there has been increased interest in the study of aerosol chemical composition and size distribution since the health

* Corresponding author.
*E-mail address:* eyubero@umh.es (E. Yubero).

https://doi.org/10.1016/j.chemosphere.2022.133693
Received 6 September 2021; Received in revised form 22 November 2021; Accepted 17 January 2022
Available online 18 January 2022

and environmental effects of atmospheric particulate matter (PM) depend on these properties (Cassee et al., 2013; Mahowald et al., 2014). On the other hand, the chemical composition and size of atmospheric PM provide information about the emission sources and atmospheric processes generating primary and secondary aerosols, respectively (Galindo et al., 2021; Hu et al., 2013; Yue et al., 2008). Finally, aerosol size and composition also play an important role in the transport and removal processes, atmospheric chemistry, radiative effects, and cloud formation processes (Bian et al., 2019).

A major fraction of PM consists of water-soluble inorganic compounds, mainly secondary inorganic ions (sulfate, nitrate and ammonium) (Galindo et al., 2020; Squizzato et al., 2013). These species, formed from the photochemical oxidation of gaseous precursors ($SO_2$, $NO_x$ and $NH_3$), are related with visibility impairment (Zhou et al., 2012) and may also play a key role in aerosol acidity, determining its effects on human health, ecosystems and materials (Squizzato et al., 2013). On the other hand, primary inorganic components can also make up a significant contribution to atmospheric PM, especially crustal species, such as calcium (Galindo et al., 2020; Shahid et al., 2019), and major sea salt components ($Na^+$ and $Cl^-$) (Chan et al., 2000; Bhugwant et al., 2013).

The multimodal distribution of atmospheric aerosol components as a function of particle size varies depending on their sources and atmospheric conditions (Huang et al., 2016; Taiwo et al., 2014). For this reason, it is important to study aerosol size distributions in different environments in order to identify source signatures of components contributing to atmospheric PM. Cascade impactors have been widely used for the determination of aerosol mass size distributions in both work places and ambient air (Crespo et al., 2012; Gupta et al., 2008; Huang et al., 2016; Segalin et al., 2017; Smolík et al., 2003). These devices allow the collection of size segregated aerosols onto filters for subsequent determination of the mass, chemical and/or physical properties (Cuccia et al., 2013; Engling et al., 2009, Samara, 2017).

Port-related activities are known to be an important source of atmospheric PM and can have a strong impact on local air quality at coastal sites (Sorte et al., 2020; Viana et al., 2014). PM emissions can be due to both maritime transport and the activity at the docks (Clemente et al., 2021; Nunes et al., 2017; Pérez et al., 2016). In spite of this, there are few works regarding the impact of harbour-related activities on aerosol mass size-distributions (Merico et al., 2020) and, to the best of our knowledge, there is not any study related to the size distribution of aerosol components.

This work is focused on the determination of the size distributions of water-soluble ionic species at the harbour of Alicante (southeastern Spain). The port is an important sector of the local economy and represents a significant source of atmospheric aerosols, accounting for about 40% of $PM_{10}$ levels (Clemente et al., 2021). The selected sampling site was on the border between the port and the city, in an area accessible to pedestrians. The results of this study would be helpful to discern specific aerosol sources based on their particle size distributions, propose effective mitigation strategies to improve air quality in the area, and reduce adverse effects of harbour activities on human health, particularly for the people who live in nearby areas.

## 2. Materials and methods

### 2.1. Measurement site

The sampling site was located within the maritime port of Alicante. The city is located on the Mediterranean coast of Spain (38°20′12.6 "N 0°29′48.2 "W) and has an area of about 200 $km^2$ and a population of 331,577 inhabitants. The area is characterized by a Mediterranean climate, with mild winters and dry warm summers. A full description of the sampling point and the main features and facilities of the port can be found in Clemente et al. (2021).

The sampler was placed less than 400 m from the main bulk material (limestone and gypsum mainly) loading and unloading docks and 500 m from the nearest inhabited area. Operations with other materials such as fertilisers, woodchips, rubber and wheat are also carried out at other docks located further away. The location of the sampling point and the main docks can be found in Fig. 1. Wind roses for the summer and winter periods are also shown. During summer the wind regime was dominated by the sea breeze circulation (S-SE), while during winter the prevailing wind blew from the SE and NW directions.

It is important to highlight that particle dispersion does not only occur during loading and unloading operations, but also during the stockpiling of the materials on the days prior to the arrival of the ships.

### 2.2. Sample collection and analysis

A total of 168 size-segregated PM samples were collected during summer and winter seasons (14 sampling days x 12 stages). The first sampling period was from 20 July to 7 August 2018 (summer), while the second sampling period was from 22 February to 7 March 2019 (winter). A 12-stage Dekati low pressure impactor (DLPI) was used to collect particles ranging from 30 nm to 10 μm (0.045, 0.086, 0.153, 0.231, 0.343, 0.591, 0.796, 1.06, 1.66, 2.68, 4.08, and 8.50 μm) (Maenhaut et al., 1996; Crespo et al., 2012). A 25 mm diameter Nucleopore® polycarbonate membrane filter with a flow rate of 11 L $min^{-1}$ was used in each stage.

PM concentrations were determined according to the procedure described in EN 12341. Each filter was stored in a humidity (50 ± 5%) and temperature (20 ± 1 °C) controlled room for 48 h before and after sampling, and then weighed on a Mettler Toledo® XP 105 balance with a sensitivity of $10^{-5}$ g. The mass concentration of each filter was obtained using the gravimetric method. After weighing, the sampled filters were kept in a refrigerator at 5–8 °C until analysis by ion chromatography.

Filters were extracted with 4 mL Milli-Q water under sonication for 30 min. The concentration of anions ($Cl^-$, $NO_3^-$, $SO_4^{2-}$ and $C_2O_4^{2-}$) was obtained by analysis with a Dionex DX-120 chromatograph, equipped with an AS11-HC ion exchange column (4 × 250 mm) and an ASRS-300 suppressor (4 mm). A 10 mM sodium hydroxide solution with a flow rate of 1 mL $min^{-1}$ was used as eluent. Cations ($Na^+$, $K^+$, $Ca^{2+}$, $Mg^{2+}$ and $NH_4^+$) were analysed with a Dionex ICS-1100 chromatograph equipped with a CS12A ion exchange column (4 × 250 mm) and a CSRS-300 suppressor (4 mm). For this analysis, 20 mM methanesulphonic acid at a flow rate of 0.7 mL $min^{-1}$ was used as eluent. More details about the IC analytical procedures can be found in Galindo et al. (2018). The detection limits (determined as three times the standard deviation) in μg $m^{-3}$ were: $Cl^-$ 0.01; $NO_3^-$ 0.06; $SO_4^{2-}$ 0.05; $C_2O_4^{2-}$ 0.002; $Na^+$ 0.01; $K^+$ 0.01; $Ca^{2+}$ 0.02; $Mg^{2+}$ 0.001; $NH_4^+$ 0.02.

Carbonate concentrations were estimated from the ionic balance, assuming that the anion deficit corresponds exclusively to this ion (Galindo and Yubero, 2017). This deficit occurred in the coarse fraction, and therefore $CO_3^{2-}$ data are only available for PM above 1 μm.

The experimental results for each analyte were inverted into smooth size distributions by the computer program MICRON (Cuccia et al., 2010; Maenhaut et al., 1996; Salma et al., 2005). The inverted data were fitted by log-normal distributions so that the mass concentrations, geometric mean aerodynamic diameters (GMAD), and geometric standard deviations (GSD) of the different modes were obtained for each size distribution.

A statistical test (Kruskal-Wallis test) was used to identify significant differences between the seasonal concentrations of the analysed compounds.

## 3. Results and discussion

### 3.1. Average mass size distribution of particulate matter

The average mass size distribution for the whole measurement period is presented in Fig. 2. The size distribution of atmospheric aerosols at the sampling site was multimodal, each mode representing

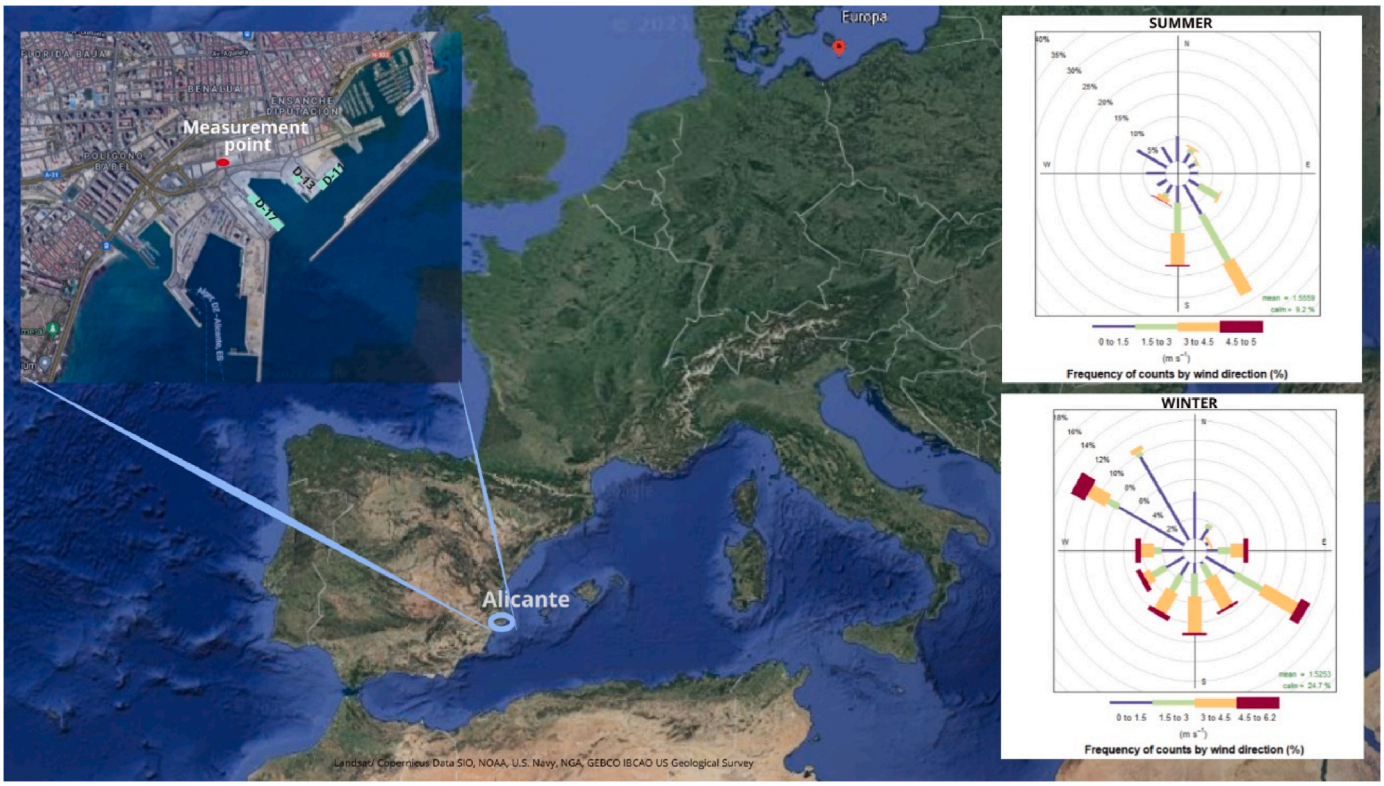


**Fig. 1.** Location of the sampling site within the port of Alicante. Summer and winter wind roses during the study period were plotted using the Openair (Carslaw and Ropkins, 2012).

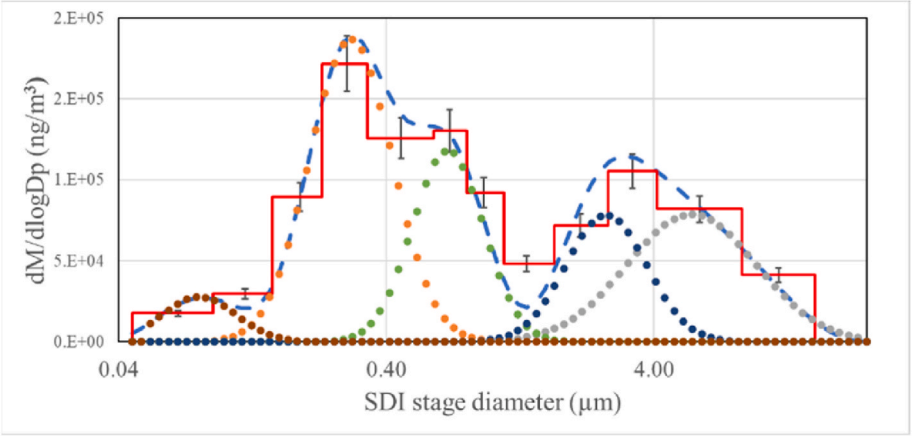


**Fig. 2.** Average aerosol mass size distribution and mode retrieval. In red, histogram of the cascade impactor experimental data; in light blue (dashed line), data inversion by the program MICRON; and in grey, blue, green and orange dots, the main modes of the distribution. (For interpretation of the references to colour in this figure legend, the reader is referred to the Web version of this article.)

different sources or formation pathways. The five modes found in this study were defined as: Aitken (<0.1 μm), condensation (between 0.1 μm and 0.5 μm), droplet (between 0.5 μm and 1 μm), coarse (between 1 μm and 5 μm), and Very Large Particles (VLP; > 5 μm). All modes were present in the whole set of samples collected during the study period, except the Aitken mode that was detected in 57% of the samples due to the limitations of the analytical procedures.

The Aitken mode (0.08 μm; 5% of the total concentration) most likely resulted from freshly emitted particles and from the growth of nucleation mode particles (Bernardoni et al., 2017; Dioni et al., 2020). Condensation-mode particles (~0.3 μm; 36% of the total concentration) could be either freshly emitted aerosols from combustion sources or secondary aerosols formed from gas-phase reactions (Bernardoni et al., 2017; Bian et al., 2014), whereas heterogeneous and aqueous-phase reactions are recognized as the main production pathways of particles in the droplet mode (~0.7 μm; 20% of the total concentration) (Wang et al., 2012; Wang et al., 2021). Finally, coarse particles (including VLP, 39% of the total concentration) could be generated by mechanical processes (sea-salt, soil dust, tire and break wear, loading and unloading activities at the docks) or correspond to aged sea-salt and dust particles (Bian et al., 2014; Seinfeld and Pandis, 2016).

### 3.2. Average size distributions of water-soluble ions

Table 1 summarizes the characteristics of the different modes for each ion. The modes found more frequently during the measurement

**Table 1**
Geometric mean aerodynamic diameter (GMAD), standard deviation (GSD), frequency of occurrence (FREQ.), and contribution of each mode to the total concentration of each ion (%total).

| | Aitken mode | | | | Condensation mode | | | | Droplet mode | | | | Coarse mode | | | | Very Large Particles mode (VLP) | | | |
|---|---|---|---|---|---|---|---|---|---|---|---|---|---|---|---|---|---|---|---|---|
| | (d < 0.1 μm) | | | | (0.1 μm < d < 0.5 μm) | | | | (0.5 μm < d < 1 μm) | | | | (1 μm < d < 5 μm) | | | | (d > 5 μm) | | | |
| | *GMAD (μm)* | *GSD* | *FREQ. (%)* | *% total* | *GMAD (μm)* | *GSD* | *FREQ. (%)* | *% total* | *GMAD (μm)* | *GSD* | *FREQ. (%)* | *% total* | *GMAD (μm)* | *GSD* | *FREQ. (%)* | *% total* | *GMAD (μm)* | *GSD* | *FREQ. (%)* | *%total (%)* |
| $Na^+$ | – | – | – | – | – | – | – | – | 0.514 | 0.093 | 100 | 14.4 | 3.875 | 0.518 | 100 | 80.3 | – | – | – | – |
| $NH_4^+$ | 0.098 | 0.036 | 85.7 | 7.3 | 0.292 | 0.027 | 100 | 54.9 | 0.578 | 0.106 | 100 | 33.1 | 2.847 | 0.470 | 100 | 3.7 | – | – | – | – |
| $Ca^{2+}$ | 0.107 | 0.034 | 71.4 | 3.4 | 0.288 | 0.054 | 100 | 5.6 | 0.811 | 0.128 | 100 | 5.9 | 4.342 | 0.710 | 100 | 72.0 | 13.081 | 2.489 | 92.9 | 13.0 |
| $K^+$ | 0.089 | 0.020 | 71.4 | 9.0 | 0.277 | 0.045 | 100 | 36.5 | 0.640 | 0.048 | 100 | 32.2 | 2.861 | 0.385 | 100 | 19.5 | – | – | – | – |
| $Mg^{2+}$ | – | – | – | – | – | – | – | – | 0.518 | 0.127 | 92.9 | 8.90 | 3.967 | 0.531 | 100 | 83.5 | – | – | – | – |
| $Cl^-$ | 0.102 | 0.037 | 85.7 | 3.3 | 0.302 | 0.085 | 100 | 5.6 | 0.751 | 0.171 | 78.6 | 5.4 | 4.265 | 0.969 | 100 | 52.9 | 9.428 | 3.359 | 92.9 | 29.9 |
| $C_2O_4^{2-}$ | – | – | – | – | 0.298 | 0.051 | 100 | 34.9 | 0.688 | 0.114 | 100 | 20.0 | 2.803 | 0.389 | 100 | 39.9 | – | – | – | – |
| $NO_3^-$ | – | – | – | – | 0.293 | 0.085 | 100 | 9.3 | 0.709 | 0.152 | 85.7 | 7.60 | 3.808 | 0.351 | 100 | 82.2 | – | – | – | – |
| $SO_4^{2-}$ | – | – | – | – | 0.304 | 0.037 | 100 | 47.5 | 0.589 | 0.057 | 100 | 29.6 | 3.478 | 0.561 | 100 | 16.6 | – | – | – | – |
| $CO_3^{2-}$ | – | – | – | – | – | – | – | – | – | – | – | – | 4.218 | 0.504 | 100 | 67.3 | 13.616 | 1.211 | 100 | 10.3 |

period were considered as the main modes for each species. The geometric mean aerodynamic diameter (GMAD), geometric standard deviation (GSD) and contribution of each mode to the total concentration of each ion (%total) are shown. The frequency (FREQ.) of occurrence for each mode was calculated considering the number of days on which the mode appeared.

Ammonium, calcium, potassium and chloride had a mode peaking at around 100 nm, which can be either large Aitken or small condensation mode. This mode contributed less than 10% to the average mass concentration of these ions. The presence of the Aitken mode for $K^+$ was most likely due to anthropogenic emissions such as those from biomass burning and other combustion sources (Bernardoni et al., 2017; Kleeman et al., 2000; Ooki et al., 2002). Ammonium chloride is formed from the reaction of gaseous $NH_3$ and HCl to initially form gaseous $NH_4Cl$ that can change to the solid phase by homogeneous nucleation or condensation onto existing particles (Nadeau et al., 2003). The formation of particles of ammonium chloride in the Aitken mode has been reported in previous studies (Saarikoski et al., 2012; Wang et al., 2015a). Regarding $Ca^{2+}$, it was mainly found in particles larger than 1 μm, as expected from its crustal origin. In fact, the size distributions of calcium in some urban environments do not even show a peak in the fine mode (Bernardoni et al., 2017; Taiwo et al., 2014). Taiwo et al. (2014) suggested that fine mode calcium may be emitted from industrial activities such as steel manufacturing. However, tunnel studies have documented a non-negligible contribution of calcium to particles in the submicron size range (Alves et al., 2015). Taking into account that there are no industries in the vicinity of our sampling site, fine calcium was most likely released from road dust and/or port activities. Very large particles were detected for calcium and carbonate, which is in agreement with the results of previous studies (Bernardoni et al., 2017). In the case of chloride, the peak in the very large mode is an artifact of the fitting procedure of the experimental data. This artifact was most likely due to differences in chloride depletion as a function of particle size. Marine aerosols can change quickly due to reactions of NaCl with acidic species (mainly $HNO_3$ and $H_2SO_4$) releasing $Cl^-$ as gaseous HCl (Ghosh et al., 2020). Chloride depletion depends on the size of sea salt particles and generally decreases with increasing particle size (Ghosh et al., 2020; Yao et al., 2003). Our findings show that the loss of chloride was lowest for the first stage of the impactor, and this led to the appearance of a very large mode for $Cl^-$ but not for $Na^+$ and $Mg^{2+}$.

Fig. 3 shows average size distributions for the analysed ions during the whole measurement period. The elements that contributed most to the condensation and droplet modes were $SO_4^{2-}$, $NH_4^+$ and, to a lesser extent, $K^+$ and $C_2O_4^{2-}$. On the other hand, $NO_3^-$, $Ca^{2+}$, $Na^+$ $Cl^-$ and $Mg^{2+}$ were mainly distributed in the coarse mode. These results are in line with other studies performed at coastal sites (Aswini and Hegde, 2021; Bougiatioti et al., 2013).

### 3.2.1. *Marine ions ($Na^+$, $Cl^-$ and $Mg^{2+}$)*

Sea salt aerosols are formed at the ocean surface by bubble-bursting and jet drops, and predominate in the coarse fraction (Bian et al., 2019; Feng et al., 2017). The size distributions of sea salt components at our sampling location had a prominent mode in the coarse fraction at ~4 μm, reflecting the proximity of the site to the Mediterranean Sea. This mode accounted for around 80% of the $Na^+$ and $Mg^{2+}$ mass concentrations. Similar findings were obtained at other coastal sites (Do et al., 2021; Feng et al., 2017; Taiwo et al., 2014). Sodium and magnesium also had a small peak in the droplet mode (~0.5 μm), which is consistent with previous works (Taiwo et al., 2014). Fine-mode sodium has been associated with anthropogenic sources rather than sea salt emissions; therefore, the contribution of the droplet mode to the total mass of sodium can be comparable to that of the coarse mode in urban areas where local anthropogenic emissions of $Na^+$ are significant (Huang et al., 2016; Zhao et al., 2011). In this study, the correlation between $Mg^{2+}$ and $Na^+$ concentrations in the size bins below 1.06 μm ($R^2 = 0.79$) points to a prevalent marine origin for both ions in the fine fraction.

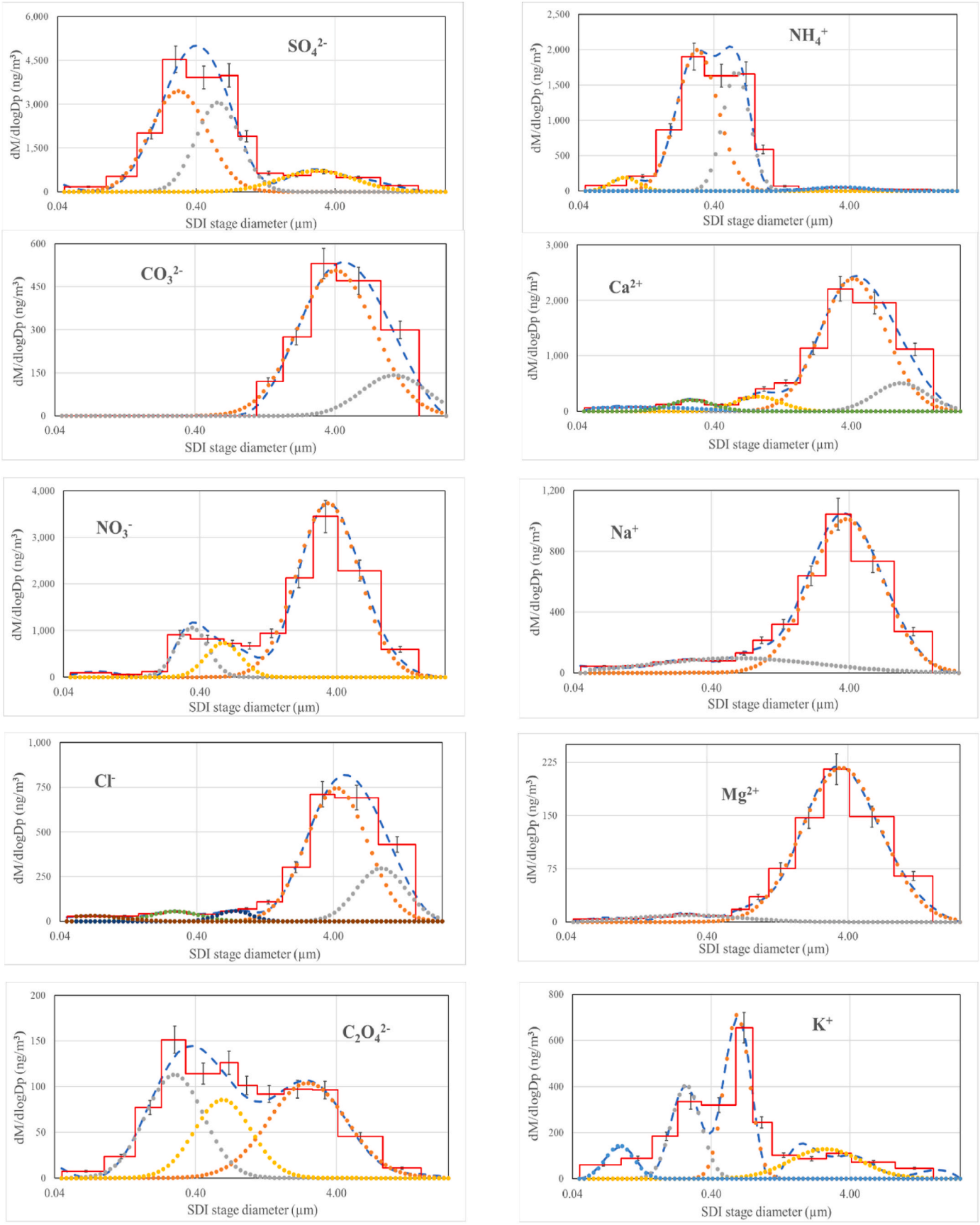


**Fig. 3.** Average size distributions for water-soluble ions and mode retrieval. In red, histogram of the cascade impactor experimental data; in blue (dashed line), data inversion by the program MICRON; and in yellow, grey, orange, blue and green dots, the main modes of the distribution. (For interpretation of the references to colour in this figure legend, the reader is referred to the Web version of this article.)

The average size distribution for $Cl^-$ was different from that of $Na^+$ and $Mg^{2+}$. As explained above, an additional peak at ~9 μm was observed as a result of chloride depletion being dependent on the particle size. Hence, we can conclude that the maximum in the very large mode is not a real peak and that the chloride distribution does not reflect the sea salt size distribution.

### 3.2.2. Secondary water-soluble ions ($SO_4^{2-}$, $NO_3^-$, $NH_4^+$ and $C_2O_4^{2-}$)

Sulfate and ammonium showed a practically bimodal distribution in the submicron size range, with peaks in the condensation and droplet modes. The condensation mode (peaking at ~ 0.3 μm) contributed around 50% to the total mass concentrations, while the droplet mode (with an average aerodynamic diameter of ~0.6 μm) accounted for approximately 30%. These modes have already been described in previous studies (Cabada et al., 2004; Guo et al., 2010; Zhuang et al., 1999) and correspond to two different formation pathways. The condensation mode for $SO_4^{2-}$ was suggested to originate from the gas-phase oxidation of $SO_2$ followed by gas-to-particle conversion (Seinfeld and Pandis, 2016), while the droplet mode results from the aqueous-phase oxidation of $SO_2$ in cloud and fog droplets mainly by $H_2O_2$ and by transition metals catalysed oxidation (Wang et al., 2021). Other processes that may explain the formation of droplet-mode sulfate include condensation and coagulation of smaller particles and the growth of the condensation mode by addition of sulfate and water (Guo et al., 2010). The dominance of particles in the condensation mode at our sampling site indicates that the formation of secondary sulfate during the study period was mainly from gas-phase reactions, most likely because sampling was performed on sunny days without low clouds (Plaza et al., 2011; Zhuang et al., 1999). The mode diameters of ammonia in the condensation and droplet size ranges were the same as those of sulfate, indicating that both ions coexist in these particles. Ammonium in fine particles is formed from the reactions of gaseous ammonia with acidic species such as $H_2SO_4$, $HNO_3$ and HCl. Since ammonium sulfate is more stable than the other ammonium salts, $NH_3$ prefers to react with sulfuric acid or sulfate. The slope of the linear regression line between $SO_4^{2-}$ and $NH_4^+$ concentrations (in μeq $m^{-3}$) in the 0.153–0.343 μm and the 0.591–1.06 μm size ranges was 0.95 ($R^2$ >0.93), pointing to the formation of $(NH_4)_2SO_4$ in both modes.

Sulfate showed a minor peak in the coarse mode at 3.4 μm, which accounted for 17% of the total sulfate. This peak has been commonly observed in several previous studies (Do et al., 2021; Plaza et al., 2011; Taiwo et al., 2014; Zhao et al., 2011; Zhuang et al., 1999) and results from the reaction of $SO_2$ or $H_2SO_4$ with coarse calcium and sodium particles. Coarse $NH_4^+$ was found in all samples, although it contributed less than 5% to the total ammonium mass concentration.

Nitrate showed a trimodal distribution; however, unlike sulfate, its average size distribution was dominated by coarse mode particles (3.8 μm), accounting for 80% of the total nitrate mass concentration. Coarse-mode nitrate is mainly formed from heterogeneous reactions of nitric acid with mineral dust and/or sea salt particles (Dasgupta et al., 2007; Hodzic et al., 2006). Two small peaks were obtained in the fine size range with average diameters in the condensation (0.3 μm) and droplet (0.7 μm) modes, similarly to other studies (Cabada et al., 2004). Nitrate in the condensation mode is generated by the gas-phase oxidation of $NO_x$ to $HNO_3$, which then reacts with ammonia to form $NH_4NO_3$. On the other hand, the formation of the droplet-mode nitrate may be the result of heterogeneous-phase reactions or the growth of condensation-mode ammonium nitrate particles (Cabada et al., 2004; Wang et al., 2021). Fine $NH_4NO_3$ is highly unstable and tends to decompose into gaseous nitric acid and ammonia under high temperatures and low relative humidity conditions. In addition, its formation is favoured at high $NH_3$ concentrations, when there is sufficient ammonia to neutralize both $H_2SO_4$ and $HNO_3$ (Do et al., 2021; Wang et al., 2015b). This may be the reason why nitrate size distributions differ depending on the meteorological conditions and the characteristics of the study area. As just mentioned, at our sampling site nitrate was mainly distributed in the coarse size fraction, in accordance with several previous studies (Barbaro et al., 2019; Bougiatioti et al., 2013; Plaza et al., 2011; Taiwo et al., 2014; Zhuang et al., 1999). This is most likely because ammonia levels are low in the study area and the formation of ammonium nitrate is limited by the availability of ammonia (Clemente et al., 2022). In contrast, other works have reported a higher abundance of nitrate in fine-mode particles (Cabada et al., 2004; Zhao et al., 2011).

Oxalic acid is the most abundant dicarboxylic acid in atmospheric aerosols, with most of it existing as oxalate. It can be directly introduced into the atmosphere by biogenic and anthropogenic sources, although the secondary formation of oxalate through photochemical oxidation of volatile organic compounds is thought to be the main source of this anion (Bian et al., 2014; Zhou et al., 2015). The size distribution of oxalate was similar to that of sulfate, although the peak in the coarse mode (40% of the total oxalate) was larger than those in the condensation (35%) and droplet modes (20%). Trimodal distributions for oxalate have been identified in previous studies (Bian et al., 2014; Huang et al., 2006). In contrast, other works have reported bimodal size distributions with peaks in the submicron and coarse size ranges (Bardouki et al., 2003; Laongsgri and Harrison, 2013; Zhao and Gao, 2008). Regardless the number of mode peaks, oxalate size distributions are usually dominated by a large droplet mode. The formation of oxalate in the droplet mode has been attributed either to in-cloud processes or gas-to-particle formation (Zhao and Gao, 2008). When the formation pathway of droplet-mode oxalate is dominated by in-cloud processes, oxalate shows a good correlation with sulfate (Huang et al., 2006; Laongsgri and Harrison, 2013). The correlations between these two ions at our sampling site will be discussed in the next section. The condensation-mode oxalate is thought (Ooki et al., 2002) to be the result of the photochemical oxidation of gaseous precursors with OH radicals and ozone, followed by condensation of the formed oxalic acid onto existing particles (Bian et al., 2014; Kawamura et al., 2007; Laongsgri and Harrison, 2013). Regarding coarse-mode oxalate, it may be formed from the reaction of gas-phase oxalic acid with sea-salt and/or soil aerosols (Bardouki et al., 2003; Huang et al., 2006; Kawamura et al., 2007). The size distribution of oxalate at our sampling site points to gas-phase reactions as the main pathway for oxalate formation. The dominant peak in the coarse mode may be attributed to the high concentrations of alkaline particles of sea salt and soil origin.

### 3.2.3. Crustal species ($Ca^{2+}$ and $CO_3^{2-}$)

Similarly to previous studies, calcium showed a multimodal size distribution, with peaks in the submicron and supermicron size ranges (Bian et al., 2014; Park and Yu, 2019). However, $Ca^{2+}$ predominated in the coarse fraction (85%) since it is mainly derived from crustal $CaCO_3$. The coarse mode (4.3 μm) contributed 72% to the total $Ca^{2+}$ and the very large mode (~13 μm) accounted for a minor fraction (13%). Fine-mode calcium (the sum of the Aitken, condensation and droplet modes) contributed only 15% to the total $Ca^{2+}$ concentration.

During the sampling days, no Saharan dust event was recorded, suggesting that local emissions were the main source of coarse $Ca^{2+}$ at the sampling site. From the size distribution of carbonate, it can be deduced that calcium in the very large mode was found as $CaCO_3$, whereas in the coarse mode it was associated, in addition to carbonate, with nitrate and sulfate.

### 3.2.4. Soluble potassium ($K^+$)

The size distribution of potassium was characterized by multiple modes since $K^+$ can be emitted by a wide variety of sources including biomass burning, combustion processes, sea-salt, soil emissions and biogenic sources (Bougiatioti et al., 2013; Do et al., 2021; Kleeman et al., 2000; Zhao and Gao, 2008). Potassium was mainly distributed in the fine fraction, following the general pattern observed in many other studies (Barbaro et al., 2019; Bernardoni et al., 2017; Bian et al., 2014; Bougiatioti et al., 2013; Do et al., 2021). The condensation (0.3 μm) and droplet (0.6 μm) modes dominated the size distributions of potassium,

with a similar contribution to the average $K^+$ concentration (37% and 32%, respectively). These fine-mode peaks are attributed to anthropogenic sources, mainly biomass burning but also other sources such as cooking or even traffic (Almeida et al., 2005; Wang et al., 2014). Potassium in the coarse mode peaked at 2.9 μm, and contributed nearly 20% to the total $K^+$. Coarse potassium is associated with mineral dust, sea salt and biogenic emissions (Bougiatioti et al., 2013; Do et al., 2021).

### 3.3. Seasonal variation of size distributions

Most of the water-soluble components showed similar mass size distributions during summer and winter (i.e. the modal peaks were the same and the relative contribution of each mode was similar during both seasons), although for some species winter and summer concentrations were statistically different (Table 2). Only nitrate and oxalate size distributions followed a different pattern during both seasons, as will be discussed below.

Sulfate concentrations were higher in summer than in winter, as previously reported for the study area (Galindo et al., 2011, 2020). This was due to the higher production rate of $H_2SO_4$ from the photochemical oxidation of $SO_2$ during the warm season. The subsequent reaction of sulfuric acid with ammonia to form $(NH_4)_2SO_4$ can explain the increase in ammonium concentrations from winter to summer.

The seasonal cycle of soluble potassium was characterized by higher concentrations in winter than in summer. As shown in the previous section, potassium was mainly distributed in the submicron fraction, indicating that $K^+$ mainly originates from combustion sources. Therefore, the increase in potassium concentrations during the cold season may be attributed to higher emission rates from sources and the lower mixing layer height. This seasonal cycle has been previously observed at other sites (Bian et al., 2014; Galon-Negru et al., 2018).

Sodium and magnesium concentrations were slightly higher in summer as a result of the prevalence of sea breezes during this season, although the seasonal differences were lower than those found in previous works performed in the study area (Galindo et al., 2011, 2020) due to the proximity of the sampling site to the sea shore. In contrast, a decrease in chloride concentrations from winter to summer was found (although this decrease was not statistically significant due to the high standard deviation in $Cl^-$ concentrations). The reason is that chloride depletion is larger in summer due to the higher ambient temperature (Galindo and Yubero, 2017).

Calcium concentrations were higher in winter than in summer. The results of previous works performed carried out in the study area indicate that the seasonal cycle of $Ca^{2+}$ varies depending on the sampling site and meteorological conditions. In the absence of precipitation and Saharan dust intrusions, winter concentrations can be higher than those registered in summer, possibly due to a decrease in the mixing layer height during the cold months (Galindo et al., 2011; Galindo and Yubero, 2017). Otherwise, calcium levels tend to be larger during summer as a consequence of increased dust resuspension and a higher frequency of African dust outbreaks (Galindo et al., 2013).

During the study period, the total concentration of oxalate was similar in summer and winter. However, when the concentrations of the submicron and coarse fractions were calculated separately, some differences were found. Fine oxalate concentrations were higher in winter than in summer (0.12 vs 0.09 μg $m^{-3}$, calculated as the sum of the impactor stages below 1.06 μm), while the opposite was observed in the coarse fraction (0.06 vs 0.09 μg $m^{-3}$, calculated as the sum of the impactor stages above 1.06 μm). The increase in the concentrations of coarse-mode oxalate during summer is clearly seen in Fig. 4. This seasonal cycle can be explained by the intense photochemical activity favouring the formation of gaseous oxalic acid followed by condensation onto coarse alkaline particles or sea salt. It has also been suggested that supermicron oxalate particles may be the result of evaporation of oxalic acid from the smaller-size particles followed by condensation onto larger particles due to their higher alkalinity (Bian et al., 2014). This may be a reason for the decrease in the concentrations of submicron oxalate during summer. The results of the correlations between oxalate and sulfate concentrations in the submicron fraction point to different formation pathways in summer and winter, at least in the droplet mode. Fairly good correlations between both ions were observed in the 0.153–0.591 μm size bins, both in summer and winter ($R^2$ of 0.48 and 0.71, respectively), probably indicating that oxalate in the condensation mode was formed from gas-phase reactions followed by condensation or/and by heterogeneous reactions on particle surfaces. On the other hand, the mass concentrations of oxalate and sulfate in 0.591–1.06 μm showed a strong correlation in winter ($R^2 = 0.74$), and no correlation in summer ($R^2 = 0.04$). These results suggest that oxalate in the droplet mode was formed by in-cloud processes during winter and by gas-to-particle conversion during the summer season, in line with the findings of Zhao and Gao (2008). They observed a good relationship between oxalate and sulfate in 0.32–0.56 μm only when the average temperature was below 20 °C. During our study period, the average daily temperature was between 28 and 31 °C in summer, and between 14 and 18 °C during winter.

The average size distributions of nitrate during summer and winter were significantly different (Fig. 5). During the winter season, $NO_3^-$ showed a trimodal size distribution, with peaks in the submicron and coarse size ranges. Coarse nitrate concentrations were higher than those of the submicrometric fraction due to the low ammonia levels in the study region.

As mentioned in the previous section, nitrate in the condensation and droplet modes is in the form of ammonium nitrate generated by gas-phase or heterogeneous reactions, respectively. It is well known that the partitioning of $NH_4NO_3$ between the gas and aerosol phase is shifted to the particle-phase under low ambient temperatures. Thus, the thermal decomposition of particulate $NH_4NO_3$ in summer explains why nitrate had a unimodal supermicron size distribution during this season.

To gain insight into the formation of coarse-mode nitrate, the mass concentrations of nitrate for the impactor stages above 1.06 μm were correlated against the excess of sodium and calcium, defined as the fraction of $Na^+$ and $Ca^{2+}$ not bound to chloride and carbonate, respectively (Nicolás et al., 2009a). Correlations were performed separately for winter and summer (Fig. 6). During summer, most of the nitrate was in the form of $NaNO_3$ as a result of the reaction of $HNO_3$ with sea salt (R1). This indicates that chloride depletion can be largely attributed to the formation of coarse-mode nitrate, as reported in several previous works (Barbaro et al., 2019; Bian et al., 2014; Ghosh et al., 2020; Zhao and Gao, 2008; Zhuang et al., 1999). The $Ca^{2+}/Na^+$ equivalent ratio during summer, although lower than in winter, was higher than unity (1.8), indicating that calcium was the dominant alkaline ion in coarse particles. Therefore, the reaction between nitric acid and sodium chloride seems to be more dependent on the ambient temperature than on the relative proportion of sodium and calcium. The results of the correlation analysis show that a significant fraction of coarse $NO_3^-$ was associated with $Ca^{2+}$ during winter, suggesting that the reaction of nitric acid with

**Table 2**
Mean concentrations of water-soluble species (μg $m^{-3}$) during summer and winter calculated as the sum of all stages of the DEKATI impactor.

| | $Cl^-$ | $NO_3^-$ | $SO_4^{2-}$ | $C_2O_4^{2-}$ | $Na^+$ | $NH_4^+$ | $K^+$ | $Mg^{2+}$ | $Ca^{2+}$ |
|---|---|---|---|---|---|---|---|---|---|
| Summer | 0.47 | 2.09[a] | 4.91[a] | 0.17 | 0.85 | 1.69[a] | 0.28[a] | 0.17 | 1.32[a] |
| Winter | 0.75 | 3.26 | 2.59 | 0.19 | 0.78 | 0.98 | 0.52 | 0.15 | 2.43 |

[a] Seasonal differences were statistically significant at the 95% confidence level.

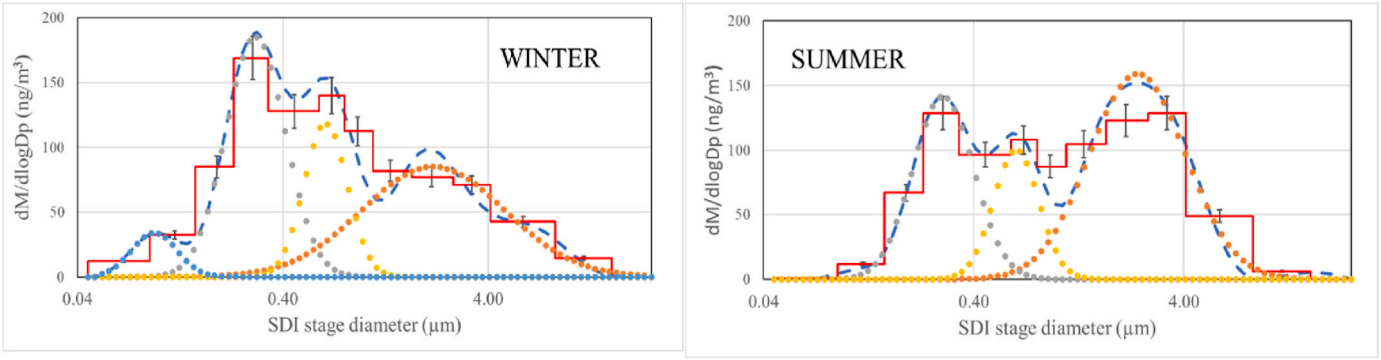


**Fig. 4.** Average size distributions of oxalate and mode retrieval during winter and summer. In red, histogram of the cascade impactor experimental data; in blue (dashed line), data inversion by the program MICRON; and in yellow, grey and orange dots, the main modes of the distribution. (For interpretation of the references to colour in this figure legend, the reader is referred to the Web version of this article.)

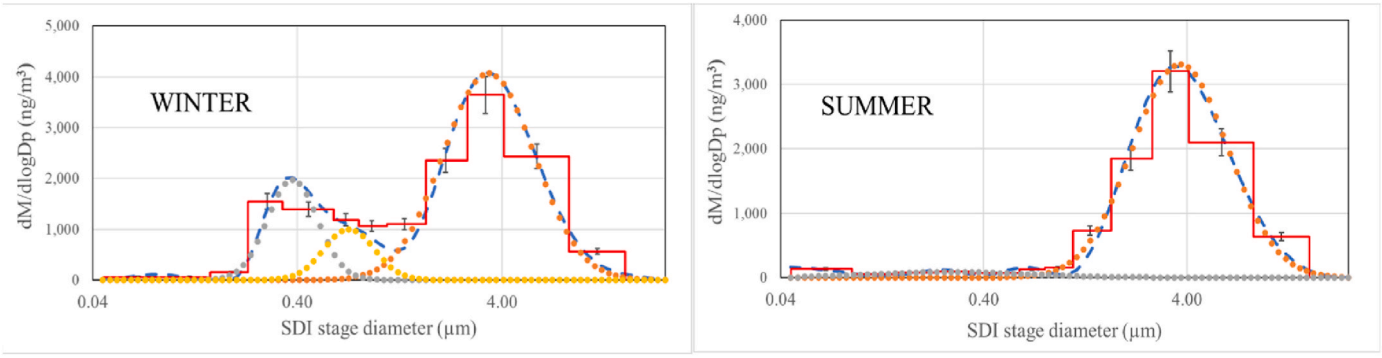


**Fig. 5.** Average size distributions of nitrate and mode retrieval during winter and summer. In red, histogram of the cascade impactor experimental data; in blue (dashed line), data inversion by the program MICRON; and in yellow, grey and orange dots, the main modes of the distribution. (For interpretation of the references to colour in this figure legend, the reader is referred to the Web version of this article.)

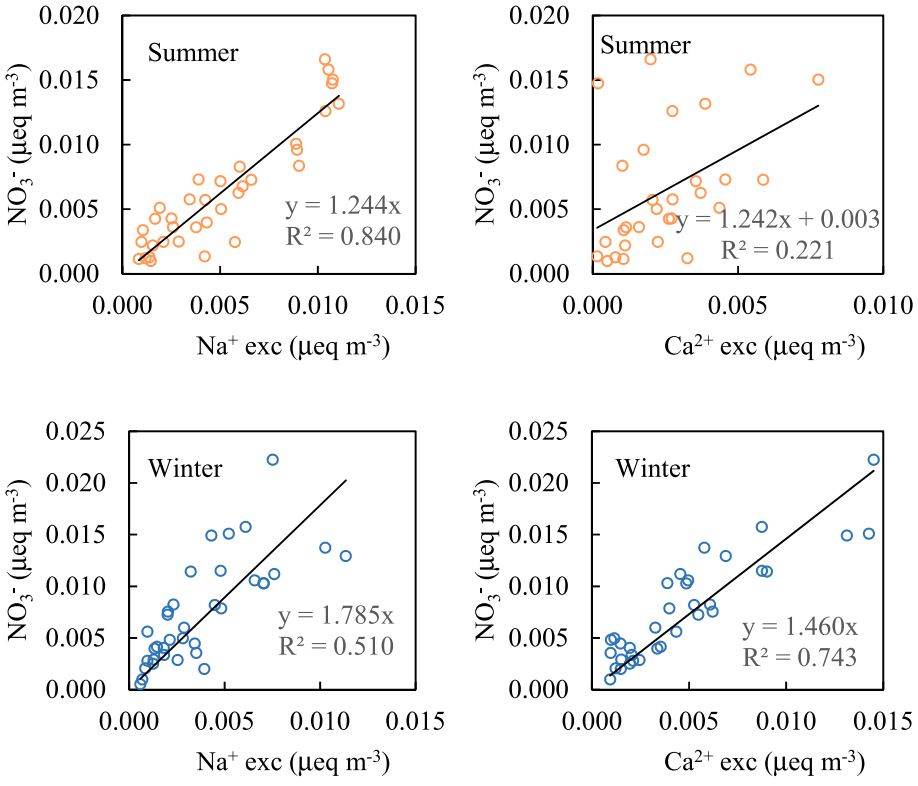


**Fig. 6.** Relationship of coarse-mode nitrate with the excess of sodium and calcium during summer and winter.

soil particles (R2) was the main pathway for coarse-mode nitrate formation during the cold season. The percentages of chloride depletion from coarse-mode sea salt aerosols, calculated using the $Cl^-/Na^+$ ratio in sea water (Ghosh et al., 2020), are in agreement with the previous outcomes since the extent of chloride deficit was higher in summer (67%) than in winter (47%). A similar seasonal pattern for chloride depletion was obtained in other works (Bian et al., 2014).

$$HNO_3\ (g) + NaCl\ (s) \rightarrow NaNO_3\ (s) + HCl\ (g) \quad (R1)$$

$$2\ HNO_3\ (g) + CaCO_3\ (s) \rightarrow Ca(NO_3)_2\ (s) + HCl\ (g) \quad (R2)$$

### 3.4. Influence of port activities on size distributions

As mentioned in Section 2.1., fugitive PM emissions can occur during both loading/unloading of cargo vessels and stockpiling of bulk materials at the docks. In order to evaluate the impact of such activities on the concentrations and size distributions of the analysed species, we first identified those days with and without port activities. For the study period, there were activities at the docks (either loading/unloading of ships, transporting or stockpiling of dust materials) during one day in summer and two days in winter. Then, we verified that not Saharan dust event was registered in order to discard any significant external influence on aerosol size distribution and composition (Nicolás et al., 2009b, 2020). Finally, the average concentrations of the studied components on the days of the study period with and without materials movement were calculated separately for winter and summer (Table 3).

The activities of loading/unloading, transporting and stockpiling of bulk materials at the docks had a clear impact on $Ca^{2+}$ levels during both summer and winter. The concentrations of soluble calcium on days with bulk materials movement were more than double those on days without these port activities during both seasons. Calcium emissions were most likely in the form of $CaCO_3$, as can be deduced from the increases in carbonate concentrations. Potassium levels showed a minor increment on days with harbour activities compared with calcium, which could suggest the presence of potassium salts in dust particles. However, this possibility is unlikely because the increase in $K^+$ concentrations was comparable or even higher in the submicron fraction. For the remaining ions, a clear influence of port activities was not observed since variations in their concentrations on days with and without bulk materials handling were different in summer and winter.

Fig. 7 presents mass size distributions for calcium on days with and without bulk port activities during summer and winter. It can be observed that, although mass concentrations on days with harbour activities were higher for all the stages, the most significant increases in $Ca^{2+}$ concentrations were generally found in the supermicron fractions, specifically on the tenth stage (mean diameter 2.68 μm).

## 4. Conclusions

Size distributions of water-soluble aerosol components ($Cl^-$, $NO_3^-$, $SO_4^{2-}$, $C_2O_4^{2-}$, $Na^+$, $K^+$, $Ca^{2+}$, $Mg^{2+}$ and $NH_4^+$) were determined at the port of Alicante during summer and winter. Sulfate and ammonium were mainly distributed in the submicron size range, with peaks in the condensation and droplet modes, suggesting the formation of $(NH_4)_2SO_4$ through both gas-phase and aqueous-phase reactions during summer and winter. Oxalate showed a trimodal size distribution with peaks in the submicron and coarse ranges. However, a higher proportion of coarse-mode oxalate was observed in summer, probably due either to the reaction of oxalic acid with sea-salt and soil derived particles or to volatilization and recondensation processes. Good correlations between oxalate and sulfate were observed in the condensation mode, pointing to similar formation pathways. In contrast, droplet-mode oxalate and sulfate were well correlated only in winter, suggesting that the formation mechanisms of oxalate in the droplet mode depend on the ambient temperature. Although the size distributions of nitrate were characterized by a dominant peak in the coarse range, two peaks in the fine mode were also observed in winter as a result of the formation of submicron $NH_4NO_3$ under low temperatures. The results of correlation analyses indicate that coarse-mode $NO_3^-$ was mostly generated from the reaction of nitric acid with soil dust during winter and sea-salt during summer. In fact, the formation of $NaNO_3$ is mainly responsible for the significant $Cl^-$ depletion.

Harbour activities (including stockpiling of bulk materials at the docks, transport, and loading/unloading of ships) had a significant influence on the levels of soluble calcium. Total $Ca^{2+}$ concentrations were more than twice higher on days with bulk materials handling than on days without materials movement during both summer and winter. Although the increase in calcium levels was observed in general for all the stages of the impactor, the highest increment was found for particles on the stage with a cutoff diameter of 2.68 μm. These results indicate that the storage and handling of bulk materials outdoors can have a significant impact on air quality in the area. Therefore, measures to minimize fugitive emissions from these activities should be taken. These measures could include outdoor storage limitations (through the building of warehouses) and proper loading/unloading methods. Other mitigation actions to be considered are: addition of water to the area of the pile being worked, use of misters and/or dry fogging systems, and daily road sweeping to minimize road dust resuspension. The temporarily suspension of operations under breeze conditions that can favour dust transport to the city, or under highly stable atmospheric conditions leading to the accumulation of pollutants in the surroundings of the port area, should also be contemplated.

## Credit author statement

B. Navarro Selma: Formal analysis, Investigation, Visualization, Writing-original draft, Writing- review and editing. A. Clemente: Formal analysis, Investigation. J.F. Nicolás: Funding acquisition, Project administration. J. Crespo: Funding acquisition, Project administration, Writing-review and editing. A. Carratalá: Conceptualization, Writing-review and editing. F. Lucarelli: Validation, resources, Writing-review and editing. N. Galindo: Writing-original draft, Supervision. E. Yubero: Conceptualization, Supervision, Writing-review and editing.

## Declaration of competing interest

The authors declare that they have no known competing financial interests or personal relationships that could have appeared to influence

**Table 3**
Mean concentrations of water-soluble species (μg $m^{-3}$) on days with and without activities at the docks (loading/unloading of vessels and/or stockpiling of bulk materials) calculated as the sum of all stages of the DEKATI impactor.

| | | $Cl^-$ | $NO_3^-$ | $SO_4^{2-}$ | $C_2O_4^{2-}$ | $CO_3^{2-}$ | $Na^+$ | $NH_4^+$ | $K^+$ | $Mg^{2+}$ | $Ca^{2+}$ |
|---|---|---|---|---|---|---|---|---|---|---|---|
| Winter | With port activities | 0.72 | 3.35 | 3.24 | 0.23 | 1.07 | 0.66 | 1.12 | 0.56 | 0.15 | 4.05 |
| | Without port activities | 0.75 | 3.23 | 2.33 | 0.17 | 0.45 | 0.86 | 0.93 | 0.50 | 0.16 | 1.78 |
| Summer | With port activities | 0.83 | 1.50 | 3.38 | 0.17 | 0.91 | 0.85 | 0.88 | 0.36 | 0.16 | 2.86 |
| | Without port activities | 0.41 | 2.19 | 5.17 | 0.15 | 0.38 | 0.85 | 1.82 | 0.27 | 0.18 | 1.06 |

*Seasonal differences were statistically significant at the 95% confidence level.

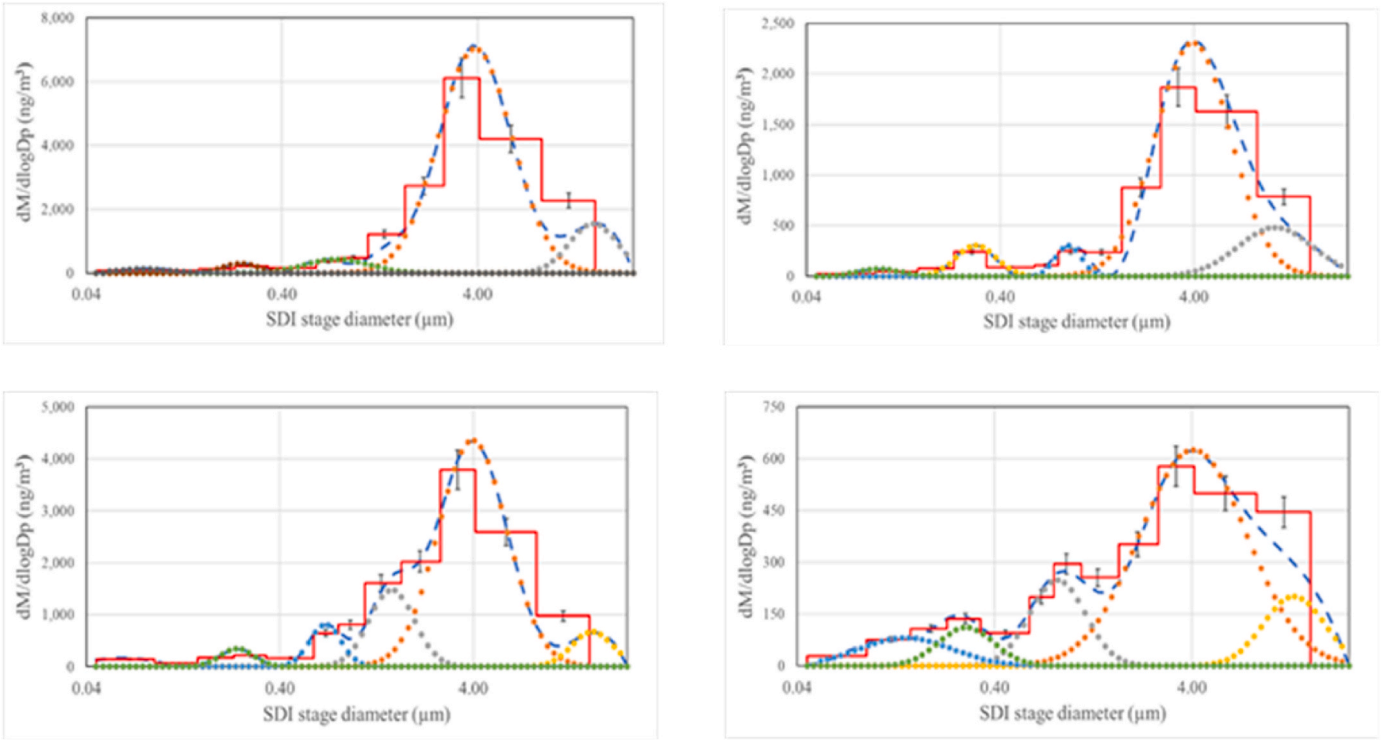


**Fig. 7.** Size distributions of $Ca^{2+}$ and mode retrieval during winter (top) and summer (bottom) on days with (left) and without (right) port activities. In red, histogram of the cascade impactor experimental data; in blue (dashed line), data inversion by the program MICRON; and in yellow, grey, orange and green dots, the main modes of the distribution. (For interpretation of the references to colour in this figure legend, the reader is referred to the Web version of this article.)

the work reported in this paper.

## Acknowledgements

We thank the Alicante Port Authority (APA) and Bergé Marítima S.L. for allowing access to their facilities, funding sampling and supplying data. This work was supported by the Spanish Ministry of Science, Innovation and Universities (COSMOS Project, ref. RTI2018-098639-B-I00). The authors would also like to thank ACTRIS-Spain network (CGL2017-90884-REDT). A. Clemente thanks the Spanish Ministry of Education for a predoctoral grant (FPU18/00081).

## References

Almeida, S.M., Pio, C.A., Freitas, M.C., Reis, M.A., Trancoso, M.A., 2005. Source apportionment of fine and coarse particulate matter in a sub-urban area at the Western European Coast. Atmos. Environ. 39, 3127–3138.
Alves, C.A., Gomes, J., Nunes, T., Duarte, M., Calvo, A., Custodio, D., Pio, C., Karanasiou, A., Querol, X., 2015. Size-segregated particulate matter and gaseous emissions from motor vehicles in a road tunnel. Atmos. Res. 153, 134–144.
Aswini, A.R., Hegde, P., 2021. Impact assessment of continental and marine air-mass on size-resolved aerosol chemical composition over coastal atmosphere: significant organic contribution in coarse mode fraction. Atmos. Res. 248, 105216.
Barbaro, E., Feltracco, M., Cesari, D., Padoan, S., Zangrando, R., Contini, D., Barbante, C., Gambaro, A., 2019. Characterization of the water soluble fraction in ultrafine, fine, and coarse atmospheric aerosol. Sci. Total Environ. 658, 1423–1439.
Bardouki, H., Liakakou, H., Economou, C., Sciare, J., Smolík, J., Ždímal, V., Eleftheriadis, K., Lazaridis, M., Dye, C., Mihalopoulos, N., 2003. Chemical composition of size-resolvedatmospheric aerosols in the eastern Mediterranean during summer and winter. Atmos. Environ. 37, 195–208.
Bernardoni, V., Elser, M., Valli, G., Valentini, S., Bigi, A., Fermo, P., Piazzalunga, A., 2017. Size-segregated aerosol in a hot-spot pollution urban area: chemical composition and three-way source apportionment. Environ. Pollut. 231, 601–611.
Bhugwant, C., Bessafi, M., Favez, O., Chiappini, L., Sieja, B., Leoz-Garziandia, E., 2013. High contribution of sea salt aerosols on atmospheric particles measured at an urban tropical location in Reunion Island. J. Environ. Protect. 4, 828–842.
Bian, Q., Huang, X.H.H., Yu, J.Z., 2014. One-year observations of size distribution characteristics of major aerosol constituents at a coastal receptor site in Hong Kong – Part 1: inorganic ions and oxalate. Atmos. Chem. Phys. 14, 9013–9027.
Bian, H., Froyd, K., Murphy, D., Dibb, J., Darmenov, A., Chin, M., Colarco, P.R., da Silva, A., Kucsera, T.L., Schill, G., Yu, H., Bui, P., Dollner, M., Weinzierl, B., Smirnov, A., 2019. Observationally constrained analysis of sea salt aerosol in the marine atmosphere. Atmos. Chem. Phys. 19, 10773–10785.
Bougiatioti, A., Zarmpas, P., Koulouri, M., Theodosi, C., Kouvarakis, C., Saarikoski, S., Mäkelä, T., Hillamo, R., Mihalopoulos, N., 2013. Organic, elemental and water-soluble organic carbon in size segregated aerosols, in the marine boundary layer of the Eastern Mediterranean. Atmos. Environ. 64, 251–262.
Cabada, J.C., Rees, S., Takahama, S., Khlystov, A., Pandis, S.N., Davidson, C.I., Robinson, A.L., 2004. Mass size distributions and size resolved chemical composition offine particulate matter at the Pittsburgh supersite. Atmos. Environ. 38, 3127–3141.
Carslaw, D.C., Ropkins, K., 2012. Openair — an R package for air quality data analysis. Environ. Model. Software 27–28, 52–61.
Cassee, F.R., Héroux, M.E., Gerlofs-Nijland, M.E., Kelly, F.J., 2013. Particulate matter beyond mass: recent health evidence on the role of fractions, chemical constituents and sources of emission. Inhal. Toxicol. 25, 802–812.
Chan, Y.C., Vowles, P.D., G, H., Simpson, R.W., Cohen, D.D., Baily, G.M., McOrist, G.D., 2000. Characterisation and source identification of $PM_{10}$ aerosol samples collected with a high volume cascade impactor in Brisbane (Australia). Sci. Total Environ. 262, 5–19.
Clemente, A., Yubero, E., Galindo, N., Crespo, J., Santacatalina, M., Carratalá, A., 2021. Quantification of the impact of port activities on $PM_{10}$ levels at the port-city boundary of a Mediterranean city. J. Environ. Manag. 281, 111842.
Clemente, A., Yubero, E., Nicolás, J.F., Caballero, S., Crespo, J., Galindo, N., 2022. Changes in the concentration and composition of urban aerosols during the COVID-19 lockdown. Environ. Res. 203, 111788.
Crespo, J., Yubero, E., Nicolás, J.F., Lucarelli, F., Nava, S., Chiari, M., Calzolai, G., 2012. High-time resolution and size-segregated elemental composition in high-intensity pyrotechnic exposures. J. Hazard Mater. 241–242, 82–91.
Cuccia, E., Bernardoni, V., Massabò, D., Prati, P., Valli, G., Vecchi, R., 2010. An alternative way to determine the size distribution of airborne particulate matter. Atmos. Environ. 44, 3304–3313.
Cuccia, E., Massabò, D., Ariola, V., Bove, M.C., Fermo, P., Piazzalunga, A., Prati, P., 2013. Size-resolved comprehensive characterization of airborne particulate matter. Atmos. Environ. 67, 14–26.
Dasgupta, P.K., Campbell, S.W., Al-Horr, R.S., Rahmat Ullah, S.M., Li, J., Amalfitano, C., Poor, N.D., 2007. Conversion of sea salt aerosol to $NaNO_3$ and the production of HCl: analysis of temporal behavior of aerosol chloride/nitrate and gaseous $HCl/HNO_3$ concentrations with AIM. Atmos. Environ. 41, 4242–4257.
Dioni, A., Conte, M., Grasso, F.M., Contini, D., 2020. Long-term characterization of submicron atmospheric particles in an urban background site in southern Italy. Atmosphere 11, 334.
Do, T.V., Vuong, Q.T., Choi, S.D., 2021. Day–night variation and size distribution of water-soluble inorganic ions in particulate matter in Ulsan, South Korea. Atmos. Res. 247, 105145.

Engling, G., Lee, J.J., Tsai, Y.W., Lung, S.C.C., Chou, C.C.K., Chan, C.Y., 2009. Size-resolved anhydrosugar composition in smoke aerosol from controlled field burning of rice straw. Aerosol Sci. Technol. 43, 662–672.
Feng, L., Shen, H., Zhu, Y., Gao, H., Yao, X., 2017. Insight into generation and evolution of sea-salt aerosols from field measurements in diversified marine and coastal atmospheres. Sci. Rep. 7, 41260.
Galindo, N., Yubero, E., Nicolás, J.F., Crespo, J., Pastor, C., Carratalá, A., Santacatalina, M., 2011. Water-soluble ions measured in fine particulate matter next to cement works. Atmos. Environ. 45, 2043–2049.
Galindo, N., Gil-Moltó, J., Varea, M., Chofre, C., Yubero, E., 2013. Seasonal and interannual trends in PM levels and associated inorganic ions in southeastern Spain. Microchem. J. 110, 81–88.
Galindo, N., Yubero, E., 2017. Day-night variability of water-soluble ions in $PM_{10}$ samples collected at a traffic site in southeastern Spain. Environ. Sci. Pollut. Res. 24, 805–812.
Galindo, N., Yubero, E., Nicolás, J.F., Varea, M., Clemente, Á., 2018. Day-night variability of $PM_{10}$ components at a Mediterranean urban site during winter. Air Qual. Atmos. Health 11, 1251–1258.
Galindo, N., Yubero, E., Clemente, Á., Nicolás, J.F., Varea, M., Crespo, J., 2020. PM events and changes in the chemical composition of urban aerosols: a case study in the western Mediterranean. Chemosphere 244, 125520.
Galindo, N., Clemente, Á., Yubero, E., Nicolás, J.F., Crespo, J., 2021. $PM_{10}$ chemical composition at a residential site in the western Mediterranean: estimation of the contribution of biomass burning from levoglucosan and its isomers. Environ. Res. 196, 110394.
Galon-Negru, A.G., Olariu, R.I., Arsene, C., 2018. Chemical characteristics of size-resolved atmospheric aerosols in Iasi, north-eastern Romania: nitrogen-containing inorganic compounds control aerosol chemistry in the area. Atmos. Chem. Phys. 18, 5879–5904.
Ghosh, A., Roy, A., Das, S.K., Ghosh, S.K., Raha, S., Chatterjee, A., 2020. Identification of most preferable reaction pathways for chloride depletion from size segregated sea-salt aerosols: a study over high altitude Himalaya, tropical urban metropolis and tropical coastal mangrove forest in eastern India. Chemosphere 245, 125673.
Gupta, S., Srivastava, A., Jain, V.K., 2008. Particle size distribution of aerosols and associated heavy metals in kitchen environments. Environ. Monit. Assess. 142, 141–148.
Guo, S., Hu, M., Wang, Z.B., Slanina, J., Zhao, Y.L., 2010. Size-resolved aerosol water-soluble ionic compositions in the summer of Beijing: implication of regional secondary formation. Atmos. Chem. Phys. 10, 947–959.
Hu, X., Ding, Z., Zhang, Y., Sun, Y., Wu, J., Chen, Y., Lian, H., 2013. Size distribution and source apportionment of airborne metallic elements in Nanjing, China. Aerosol Air Qual. Res. 13, 1796–1806.
Huang, X.F., Yu, J.Z., He, L.Y., Yuan, Z., 2006. Water-soluble organic carbon and oxalate in aerosols at a coastal urban site in China: size distribution characteristics, sources, and formation mechanisms. J. Geophys. Res. 111, D22212.
Huang, X., Liu, Z., Zhang, J., Wen, T., Ji, D., Wang, Y., 2016. Seasonal variation and secondary formation of size-segregated aerosol water-soluble inorganic ions during pollution episodes in Beijing. Atmos. Res. 168, 70–79.
Hodzic, A., Bessagnet, B., Vautard, R., 2006. A model evaluation of coarse-mode nitrate heterogeneous formation on dust particles. Atmos. Environ. 40, 4158–4171.
Kawamura, K., Narukawa, M., Li, S.M., Barrie, L.A., 2007. Size distributions of dicarboxylic acids and inorganic ions in atmospheric aerosols collected during polar sunrise in the Canadian high Arctic. J. Geophys. Res. 112, D10307.
Kleeman, M.J., Schauer, J.J., Cass, G.R., 2000. Size and composition distribution of fine particulate matter emitted from motor vehicles. Environ. Sci. Technol. 34, 1132–1142.
Laongsgri, B., Harrison, R.M., 2013. Atmospheric behaviour of particulate oxalate at UK urban background and rural sites. Atmos. Environ. 71, 319–326.
Mahowald, N., Albani, S., Kok, J.F., Engelstaeder, S., Scanza, R., Ward, D.S., Flanner, M. G., 2014. The size distribution of desert dust aerosols and its impact on the Earth system. Aeolian Res. 15, 53–71.
Maenhaut, W., Hillamo, R., Mäkelä, T., Jaffrezo, J.-L., Bergin, M.H., Davidson, C.I., 1996. A new cascade impactor for aerosol sampling with subsequent PIXE analysis. Nucl. Instrum. Methods Phys. Res. B 109–110, 482–487.
Merico, E., Conte, M., Grasso, F.M., Cesari, D., Gambaro, A., Morabito, E., Gregoris, E., Orlando, S., Alebić-Juretić, A., Zubak, V., Mifka, B., Contini, D., 2020. Comparison of the impact of ships to size-segregated particle concentrations in two harbour cities of northern Adriatic Sea. Environ. Pollut. 266, 115175.
Nadeau, P., Berk, D., Munz, R.J., 2003. Ammonium chloride aerosol nucleation and growth in a cross-flow impinging jet reactor. Aerosol Sci. Technol. 37, 82–95.
Nicolás, J.F., Galindo, N., Yubero, E., Pastor, C., Esclapez, R., Crespo, J., 2009a. Aerosol inorganic ions in a semiarid region on the southeastern Spanish Mediterranean coast. Water Air Soil Pollut. 201, 149–159.
Nicolás, J.F., Yubero, E., Galindo, N., Giménez, J., Castañer, R., Carratalá, A., Crespo, J., Pastor, C., 2009b. Characterization of events by aerosol mass size distributions. J. Environ. Monit. 11, 394–399.
Nicolás, J.F., Lucarelli, F., Galindo, N., Yubero, E., Crespo, J., Calzolai, G., Nava, S., 2020. Impact of traffic flows and meteorological events on the hourly elemental composition of fine and coarse particles at an urban site. Aerosol Air Qual. Res. 20, 991–1001.
Nunes, R.A.O., Alvim-Ferraz, M.C.M., Martins, F.G., Sousa, S.I.V., 2017. Assessment of shipping emissions on four ports of Portugal. Environ. Pollut. 231, 1370–1379.
Ooki, A., Uematsu, M., Miura, K., Nakae, S., 2002. Sources of sodium in atmospheric fine particles. Atmos. Environ. 36, 4367–4374.
Park, S., Yu, G.H., 2019. Absorption properties and size distribution of aerosol particles during the fall season at an urban site of Gwangju, Korea. Environ. Eng. Res. 24, 159–172.
Pérez, N., Pey, J., Reche, C., Cortés, J., Alastuey, A., Querol, X., 2016. Impact of harbour emissions on ambient PM10 and PM2.5 in Barcelona (Spain): Evidences of secondary aerosol formation within the urban area. Sci. Total Environ. 571, 237–250.
Plaza, J., Pujadas, M., Gómez-Moreno, F.J., Sánchez, M., Artíñano, B., 2011. Mass size distributions of soluble sulfate, nitrate and ammonium in the Madrid urban aerosol. Atmos. Environ. 45, 4966–4976.
Saarikoski, S., Carbone, S., Decesari, S., Giulianelli, L., Angelini, F., Canagaratna, M., Ng, N.L., Trimborn, A., Faccini, M.C., Fuzzi, S., Hillamo, R., Worsnop, D., 2012. Chemical characterization of springtime submicrometer aerosol in Po Valley, Italy. Atmos. Chem. Phys. 12, 8401–8421.
Salma, I., Ocskay, R., Raes, N., Maenhaut, W., 2005. Fine structure of mass size distributions in an urban environment. Atmos. Environ. 39, 5363–5374.
Samara, C., 2017. On the redox activity of urban aerosol particles: implications for size distribution and relationships with organic aerosol components. Atmosphere 8, 205.
Segalin, B., Kumar, P., Micadei, K., Fornaro, A., Gonçalves, F.L.T., 2017. Size-segregated particulate matter inside residences of elderly in the metropolitan area of São Paulo, Brazil. Atmos. Environ. 148, 139–141.
Seinfeld, J.H., Pandis, S.N., 2016. Atmospheric Chemistry and Physics: from Air Pollution to Climate Change, third ed. John Wiley & Sons.
Shahid, I., Kistler, M., Shahid, M.Z., Puxbaum, H., 2019. Aerosol chemical characterization and contribution of biomass burning to particulate matter at a residential site in Islamabad, Pakistan. Aerosol Air Qual. Res. 19, 148–162.
Smolík, J., Ždímal, V., Schwarz, J., Lazaridis, M., Havránek, V., Eleftheriadis, K., Mihalopoulos, N., Bryant, C., Colbeck, I., 2003. Size resolved mass concentration and elemental composition of atmospheric aerosols over the Eastern Mediterranean area. Atmos. Chem. Phys. 3, 2207–2216.
Sorte, S., Rodrigues, V., Borrego, C., Monteiro, A., 2020. Impact of harbour activities on local air quality: a review. Environ. Pollut. 257, 113542.
Squizzato, S., Masiol, M., Brunelli, A., Pistollato, S., Tarabotti, E., Rampazzo, G., Pavoni, B., 2013. Factors determining the formation of secondary inorganic aerosols: a case study in the Po Valley (Italy). Atmos. Chem. Phys. 13, 1927–1939.
Taiwo, A.M., Beddows, D.C.S., Shi, Z., Harrison, R.M., 2014. Mass and number size distributions of particulate matter components: comparison of an industrial site and an urban background site. Sci. Total Environ. 475, 29–38.
Viana, M., Hammingh, P., Colette, A., Querol, X., Degraeuwe, B., de Viegler, I., van Aardenne, J., 2014. Impact of maritime transport emissions on coastal air quality in Europe. Atmos. Environ. 90, 96–105.
Wang, X., Wang, W., Yang, L., Gao, X., Nie, W., Yu, Y., Xu, P., Zhou, Y., Wang, Z., 2012. The secondary formation of inorganic aerosols in the droplet mode through heterogeneous aqueous reactions under haze conditions. Atmos. Environ. 63, 68–76.
Wang, W., Maenhaut, W., Yang, W., Liu, X., Bai, Z., Zhang, T., Claeys, M., Cachier, H., Dong, S., Wang, Y., 2014. One–year aerosol characterization study for $PM_{2.5}$ and $PM_{10}$ in Beijing. Atmos. Pollut. Res. 5, 554–562.
Wang, Y.H., Liu, Z.R., Zhang, J.K., Hu, B., Ji, D.S., Yu, Y.C., Wang, Y.S., 2015a. Aerosol physicochemical properties and implications for visibility during an intense haze episode during winter in Beijing. Atmos. Chem. Phys. 15, 3205–3215.
Wang, S., Nan, J., Shi, C., Fu, Q., Gao, S., Wang, D., Cui, H., Saiz-Lopez, A., Zhou, B., 2015b. Atmospheric ammonia and its impacts on regional air quality over the megacity of Shanghai, China. Sci. Rep. 5, 15842.
Wang, S., Wang, L., Wang, N., Ma, S., Su, F., 2021. Formation of droplet-mode secondary inorganic aerosol dominated the increased $PM_{2.5}$ during both local and transport haze episodes in Zhengzhou, China. Chemosphere 269, 128744.
Yao, X., Fang, M., Chan, C.K., 2003. The size dependence of chloride depletion in fine and coarse sea-salt particles. Atmos. Environ. 37, 743–751.
Yue, W., Stölzel, M., Cyrys, J., Pitz, M., Heinrich, J., Kreyling, W.G., Wichmann, H.E., Peters, A., Wang, S., Hopke, P.K., 2008. Source apportionment of ambient fine particle size distribution using positive matrix factorization in Erfurt, Germany. Sci. Total Environ. 398, 133–144.
Zhao, Y., Gao, Y., 2008. Mass size distributions of water-soluble inorganic and organic ions in size-segregated aerosols over metropolitan Newark in the US east coast. Atmos. Environ. 42, 4063–4078.
Zhao, J., Zhang, F., Xu, Y., Chen, J., 2011. Characterization of water-soluble inorganic ions in size-segregated aerosols in coastal city, Xiamen. Atmos. Res. 99, 546–562.
Zhou, J., Zhang, R., Cao, J., Chow, J.C., Watson, J.G., 2012. Carbonaceous and ionic components of atmospheric fine particles in Beijing and their impact on atmospheric visibility. Aerosol Air Qual. Res. 12, 492–502.
Zhou, Y., Huang, X.H., Bian, Q., Griffith, S.M., Louie, P.K.K., Yu, J.Z., 2015. Sources and atmospheric processes impacting oxalate at a suburban coastal site in Hong Kong: insights inferred from 1 year hourly measurements. J. Geophys. Res. Atmos. 120, 9772–9788.
Zhuang, H., Chan, C.K., Fang, M., Wexler, A.S., 1999. Size distributions of particulate sulfate, nitrate, and ammonium at a coastal site in Hong Kong. Atmos. Environ. 33, 843–853.